Pergamon

Acta mater. 48 (2000) 4813–4825

Acta MATERIALIA

www.elsevier.com/locate/actamat

THREE DIMENSIONAL MONTE CARLO SIMULATION OF GRAIN GROWTH DURING GTA WELDING OF TITANIUM

Z. YANG[1], S. SISTA[1], J. W. ELMER[2] and T. DEBROY[1]*

[1]Department of Material Science and Engineering, The Pennsylvania State University, University Park, PA 16802-5006, USA and [2]Chemistry and Materials Science Department, Lawrence Livermore National Laboratory, Livermore, CA 94551, USA

(Received 7 March 2000; received in revised form 21 July 2000; accepted 3 August 2000)

Abstract—The work reported here represents significant advancement in the modeling of grain structure evolution in metallic systems. Utilizing computed temperature fields from a well tested heat transfer and fluid flow model, the evolution of grain structure was simulated for the first time using a three dimensional (3D) Monte Carlo model of grain growth in the heat affected zone of commercially pure titanium welds. The computed weld geometry and the simulated mean prior β grain size for different heat inputs agreed well with the corresponding experimental results when turbulence in the weld pool was considered. The grain sizes at various locations equidistant from the fusion line were different, indicating that the results of previous 2D calculations need to be reexamined. The computed grain size distribution agreed well with the corresponding experimental data. The agreement indicates significant promise for understanding grain growth in the entire heat-affected zone using a comprehensive phenomenological model. © *2000 Acta Metallurgica Inc. Published by Elsevier Science Ltd. All rights reserved.*

Keywords: Grain growth; Theory & modeling; Monte Carlo simulation; Titanium; Welding

1. INTRODUCTION

Grain structure affects the strength, toughness, ductility and corrosion resistance of alloys [1]. In the last decade, significant progress has been made in quantitative understanding of grain growth by using computer simulation techniques. In particular, the Monte Carlo (MC) technique has been applied to simulate grain growth under isothermal conditions in both two and three dimensions [2–5]. Apart from grain growth, MC simulations also provide information on the topological features of grains that cannot be obtained from analytical equations [2–4]. Recently, the MC technique has also been applied to simulate grain growth [1, 6–8] in the heat affected zone (HAZ) of a weldment in two dimensions.

In recent years considerable advancements have also been made in quantitative understanding of fusion welding processes [10, 11]. Significant progress has been made to understand the development of weld pool shape and size [12–17], cooling rate [18], and the loss of volatile alloying elements from the weld pool [19, 20]. However, efforts to quantitatively model the development of weldment microstructures starting from fundamentals of transport phenomena are just beginning [21–23, 30]. Accurate calculation of the geometry and thermal cycles in the weldment requires a well tested numerical thermofluid model. In the past decade, several numerical thermofluid models [12–16] have been established to study heat transfer and fluid flow in the arc welding processes, in which laminar flow was assumed in the weld pool. However, recent experimental observations [24] and theoretical calculations [25, 26] in gas–tungsten–arc (GTA) welding have indicated that, in many cases, the heat transfer and fluid flow in the weld pool are turbulent in nature. Previous results [25, 26] strongly suggest that accurate predictions of temperature and velocity fields in the weld pool geometry will only be possible if the effects of turbulence are modeled accurately.

There are two important deficiencies in the previous MC simulations of grain growth in welds which are addressed here. First, the previous simulations of grain growth in the HAZ of weldments were two dimensional (2D) in what really is a 3D HAZ. It will be shown here that 2D calculations of grain growth in the HAZ can lead to significant inaccuracies. Second, in previous works, the temperature fields used to simulate the grain growth were calculated from the solution of the heat conduction equation [9]. During fusion welding, liquid material circulates rapidly in the weld pool and the resulting Peclet number

* To whom all correspondence should be addressed. Tel.: +1-814-865-1974; Fax: +1-814-865-2917.

1359-6454/00/$20.00 © 2000 Acta Metallurgica Inc. Published by Elsevier Science Ltd. All rights reserved.
PII: S1359-6454(00)00279-2

for heat transfer is much larger than unity in most cases. Thus, the temperature profiles in a weldment cannot be accurately predicted from the heat conduction equation in most conditions. A mathematical model that considers convective heat transport in the weld pool is needed for accurate calculation of the thermal cycles in the weldment.

There are considerable computational challenges in conducting meaningful MC calculations. The main challenge is in the processing of a large volume of data in a realistic time frame. For example, the simulation in 400×200 2D system considering 200 MC simulation steps involves 16 million (400×200×200) data points. For a more realistic simulation, a 3D calculation with 400×200×160 grid points undergoing 200 iteration steps increases the number of data points up to about 2.6 billion. This two order of magnitude increase in volume of data presents several interesting challenges even for the most powerful modern computers. Only in recent years have such large scale computations become tractable because of advances in computational hardware. In particular, modern data visualization techniques and tools have to be pushed to their limits just to visualize the computed results even in an efficient binary format.

Here we report the first comprehensive attempt to develop a 3D model to simulate grain growth in the HAZ of a commercially pure titanium weldment during GTA welding. The temperature profiles necessary for the MC model are obtained from a well tested, 3D, turbulent heat transfer and fluid flow model [16, 23, 30]. The MC model predictions are then compared with corresponding experimental results of grain growth for welds made with various heat inputs.

2. EXPERIMENTAL PROCEDURE

A grade 2 commercially pure titanium bar of 10.2 cm diameter was welded by GTA welding. The composition of the as-received bar was (in wt%): 0.14% Fe, 0.17% O, 0.03% Al, 0.02% Cr, 0.08% C, 0.001% H, 0.014% N, 0.02% Ni, 0.005% V, and 0.004% Si. GTA welds were made at a constant power of 1.9 kW (100 A, 19 V), and extra high purity helium (99.999%) was used as both the welding and shielding gas. The titanium bar was rotated at a constant speed below the fixed electrode. Additional details about the welding procedure are available in the literature [28]. The welding conditions are listed in Table 1. In the present study, four welds at different heat inputs were examined. Different heat inputs were obtained by changing the welding speed while keeping other parameters unchanged.

2.1. Material characterization

Optical metallography was performed on post-weld samples using conventional polishing and etching techniques. Etching was performed in a chemical bath of 15 parts lactic acid, 5 parts nitric acid and 1 part hydrofluoric acid. To quantitatively describe the grain size gradient in the HAZ, the mean prior β grain sizes at various distances from the fusion line were measured using the lineal intercept method [29] by placing test lines parallel to the fusion line. Owing to a significant grain size gradient in the HAZ, different magnifications in the range 20× to 100× were used depending on the locations from the fusion line to ensure accurate grain size measurements.

3. MATHEMATICAL MODELING

3.1. Calculation of temperature field and thermal cycles

The temperature fields and thermal cycles under various welding conditions were calculated by the 3D turbulent heat transfer and fluid flow model. Detailed description of the model is given elsewhere [16, 23, 30]. The dimensions of the solution domain were 320 mm (length)×63 mm (width)×51 mm (thickness). A 56×30×25 grid system was used in the calculations. Spatially non-uniform grids were used for maximum resolution of variables. Finer grids were used near the heat source. The minimum grid spacing was 0.005 cm directly below the weld pool surface. The thermophysical properties of the titanium for calculation of the heat transfer and fluid flow are given in Table 2. The geometry of the FZ and the HAZ were predicted from the calculated temperature field. The calculated thermal cycles at various locations in the HAZ were used for modeling grain growth.

3.2. Modeling grain growth in the HAZ

3.2.1. MC simulation model. The application of the MC technique to model grain growth has been described in detail in the literature [1–8]. Only the salient features pertinent to the specific problem addressed in this paper are described here. Each grid point is assigned a random orientation number between 1 and q, where q is the total number of grain

Table 1. Welding conditions[a]

Weld no.	Speed (mm/s)	Current (A)	Voltage (V)	Power (W)	Energy per length (J/mm)
1	0.5	108	18.2	1966	3932
2	1.0	108	18.5	1998	1998
3	2.0	108	19.0	2052	1026
4	4.0	108	19.8	2138	534

[a] No preheat for all of the welds.

Table 2. Data used for the calculation of velocity and temperature fields in titanium welds

Physical property	Value
Liquidus temperature (K)	1941
Solidus temperature (K)	1941
Density of liquid metal (kg/m^3)	4400
Viscosity of liquid (kg/m s)	5.2×10^{-3}
Thermal conductivity of solid (J/m s K)	28
Thermal conductivity of liquid (J/m s K)	28[a]
Specific heat of solid (J/kg K)	700
Specific heat of liquid (J/kg K)	800
Latent heat of melting (J/kg)	292.6×10^3
Temperature coefficient of surface tension (N/m K)	-0.26×10^{-3}
Thermal expansion coefficient (K^{-1})	1.7×10^{-6}

[a] Estimated since no values are available for these data in the literature.

orientations. A grain boundary segment is defined to lie between two sites of unlike orientation. In other words, two adjacent grid points having the same orientation number are considered to be a part of the same grain. The grain boundary energy is specified by defining an interaction between nearest neighbor lattice sites. The local interaction energy, E, is calculated by the Hamiltonian:

$$E = -J\sum_{j=1}^{n}(\delta S_i S_j - 1) \tag{1}$$

where J is a positive constant which sets the scale of the grain boundary energy, δ is Kronecker's delta function, S_i is the orientation at a randomly selected site i, S_j are the orientations of its nearest neighbors, and n is the total number of the nearest neighbor sites. The sum is taken over all nearest neighbors. Each pair of nearest neighbor contributes J to the system energy when they are of unlike orientation and zero otherwise.

The kinetics of grain boundary migration are simulated by selecting a site randomly and changing its orientation to one of the nearest neighbor orientations based on energy change due to the attempted orientation change. The probability of orientation change is defined as [2]:

$$p = 1 \text{ for } \Delta E \leq 0 \tag{2}$$

$$p = e^{-\frac{\Delta E}{k_B T}} \text{ for } \Delta E \geq 0 \tag{3}$$

where ΔE is the change of energy due to the change of orientation, k_B is the Boltzman constant and T is the temperature. Thus, any successful reorientation of a grain to orientations of nearest neighbor grains corresponds to boundary migration.

Through the MC simulation, an empirical relation between the simulated grain size and the MC simulation time can be obtained as [1, 6]:

$$L = K_1 \times \lambda \times (t_{MCS})^{n_1} \tag{4}$$

which can be written as:

$$\log\left(\frac{L}{\lambda}\right) = \log(K_1) + n_1 \log(t_{MCS}) \tag{5}$$

where L is the simulated grain size measured by mean grain intercepts, λ is the discrete grid point spacing in the MC technique, t_{MCS} is the MC simulation time or MC simulation iteration steps, K_1 and n_1 are the model constants, which are obtained by regression analysis of the data generated from MC simulation. It should be noted that equation (4) represents the intrinsic grain growth kinetics of the MC model dependent only on the grid system of the MC model and largely independent of material properties and temperature–time history. The material properties are incorporated into the MC calculations as discussed below. The MC simulation time (t_{MCS}) in equation (4) is a dimensionless quantity.

3.2.2. Application to the HAZ of real welds. The grain growth in the HAZ of the welds was simulated by coupling the 3D Monte Carlo model with the 3D heat transfer and fluid flow model. Previous work on modeling grain growth in the weld HAZ using MC simulation included two approaches in relating the t_{MCS} with the real time. Radhakrishnan and Zacharia [7] and Wilson *et al.* [8] modeled grain growth in the weld HAZ considering a linear relationship between t_{MCS} and real time. Gao *et al.* [1, 6] suggested that there was no sufficient evidence to show that the MC simulation time could be linearly related to the real time in all material systems. They proposed three models, the atomistic model, the experimental data based (EDB) model and the grain boundary migration (GBM) model to relate t_{MCS} and real time to address various situations. The atomistic model is not suitable for the present simulation since the size of the simulated domain is considerably larger than the atomic scale. In addition, the EDB model can not be used in

Table 3. Data used for the calculation of the grain growth kinetics in single β phase region

Initial average grain size, L_0	25 μm
Activation enthalpy for grain growth, Q	1.02×10^5 J/mol
Grain boundary energy, γ	0.75 J/m^2
Accommodation probability, A	1.0
Average number per unit area at grain boundary, Z	2.0×10^{19} atoms/m^2
Atomic molar volume, V_m	1.1×10^{-5} m^3/mol
Activation entropy, ΔS_a	7.21 J/mol/K
Avagadro's number, N_a	6.02×10^{23}/mol
Planck's constant, h	6.624×10^{-34} J s
Lattice point spacing, λ	50 μm in the first grid system, 25 μm in the second grid system

this study because the isothermal grain growth data for the commercially pure titanium are insufficient. The experimental data for isothermal grain growth in the β-phase region of the commercially pure titanium were limited to two temperatures (1000°C and 1100°C) in the literature [31]. Therefore, the GBM was used in the present study to establish the relation between the t_{MCS} and the real time. In the GBM model, grain growth is assumed to obey a parabolic relationship, i.e. the grain growth exponent is taken as the ideal value of 0.5. The soundness of using the GBM model to simulate grain growth in commercially pure titanium can be justified by the available isothermal grain growth kinetic data in the literature, in which the grain growth exponent was found [31] to be approximately 0.5 in the β-Ti phase region within the 1000 to 1100°C range.

The relation between t_{MCS} and real time in the GBM model has been derived from fundamentals by Gao and Thompson [1] as:

$$(t_{MCS})^{2n_1} = \left(\frac{L_o}{K_1\lambda}\right)^2 + \frac{\left\{\frac{4\gamma AZV_m^2}{N_a^2 h}\times e^{\frac{\Delta S}{R^a}}\right\}}{(K_1\lambda)^2}\sum_{i=1}^{m}\left[\Delta t_i \times e^{-\frac{Q}{RT_i}}\right] \quad (6)$$

where L is the average grain size at time t, L_o is the initial average grain size, γ is the grain boundary energy, A is the accommodation probability, Z is the average number of atoms per unit area at the grain

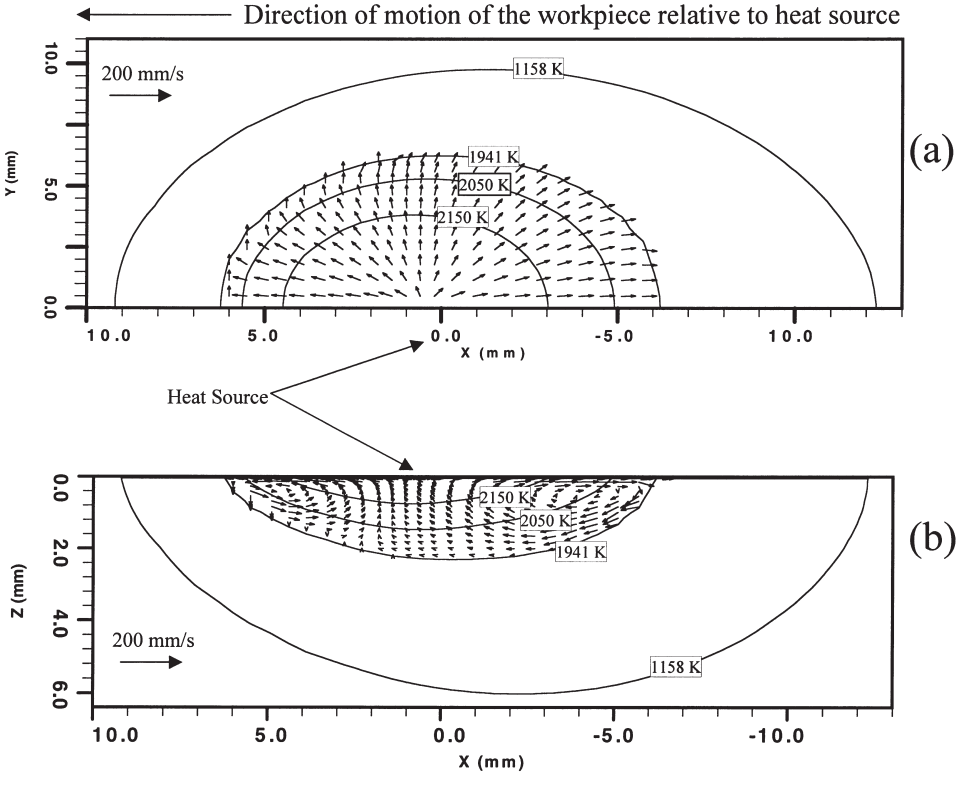

Fig. 1. Calculated temperature and velocity fields on the (a) top surface and (b) central vertical plane of weld 2 from turbulent flow model. Welding conditions: 108 A, 18.5 V and 1.0 mm/s welding speed.

Table 4. Comparison of temperatures and velocities from laminar and turbulent flow models

	Laminar model				Turbulent model			
Weld no.	Umax (mm/s)	Vmax (mm/s)	Wmax (mm/s)	Tpeak (K)	Umax (mm/s)	Vmax (mm/s)	Wmax (mm/s)	Tpeak (K)
1	36.5	102.5	14.0	2795	22.4	69.4	8.4	2429
2	29.7	86.7	11.5	2702	20.5	43.8	6.2	2295
3	25.8	59.1	7.9	2632	17.8	41.3	5.0	2207
4	23.5	55.6	5.7	2581	16.3	37.5	4.5	2144

boundary, V_m is the atomic molar volume, N_a is Avagadro's number, h is Planck's constant, ΔS_a is the activation entropy, Q is the activation enthalpy for grain growth, T is the absolute temperature, R is the gas constant and t is time. The values of the variables used in the calculations are summarized in Table 3.

The values of t_{MCS} at various locations can be calculated using equation (6) by considering the effects of the thermal cycles and material properties. In the present simulation, the initial β-Ti grain size, L_o, was assumed to be equal to the α-Ti grain size after recrystallization [28] (25 μm). Although this assumption does not consider the grain size change due to the α→β transformation, it sets an upper limit to the starting β-Ti grain size since the size of the daughter phase is less than that of the parent phase. The value of activation enthalpy, Q, for grain growth usually ranges from 1/2 to 2/3 of that for bulk diffusion [32]. Here we have taken 2/3 of the activation energy of Ti atom bulk diffusion [27, 33] (153.0 kJ/mol) as the value of that for grain growth. The grain boundary energy has been assumed to be a constant and independent of temperature [1–8]. The data for titanium grain boundary energy is not available in the literature, but was estimated [30] to be 0.75 J/m^2. The value of V_m can be calculated based on the density and atomic weight of titanium. The activation entropy for grain boundary migration, ΔS_a, can be assumed [1] to be equal to the entropy of fusion of the material, ΔS_f. The value of ΔS_a for titanium [34] is 7.21 J/mol/K. The data used for modeling grain growth are listed in Table 3.

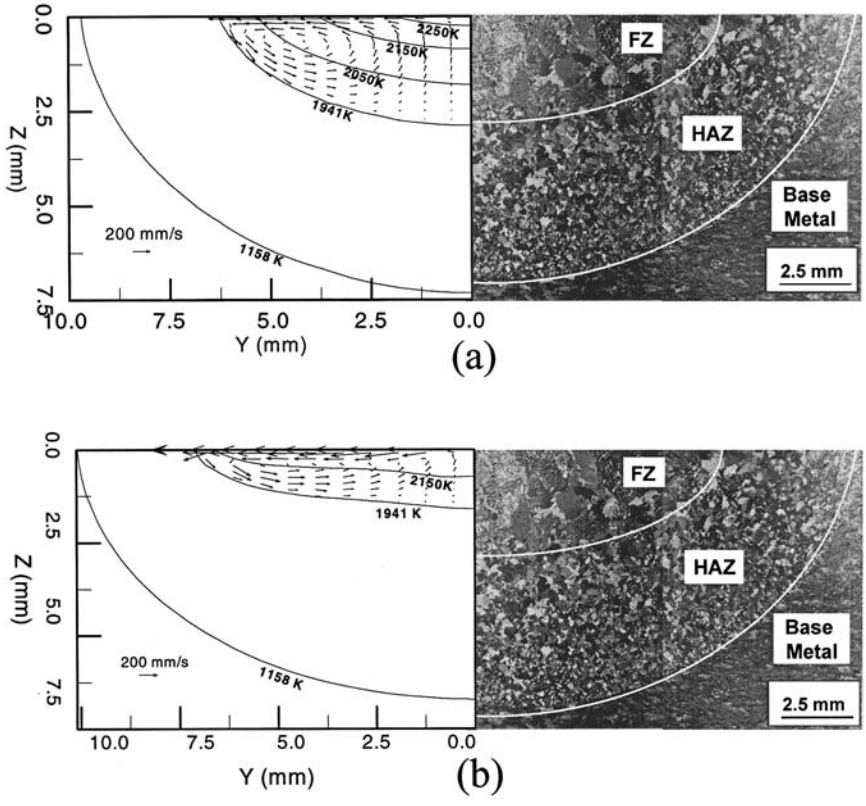

Fig. 2. Comparison of the calculated and experimental geometries for a GTA weld from (a) turbulent flow model and (b) laminar flow model. Welding conditions: 108 A, 18.5 V and 1.0 mm/s welding speed.

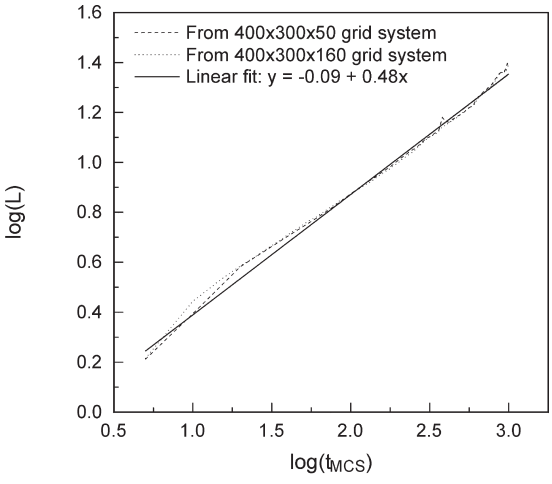

Fig. 3. Simulated grain growth kinetics from the MC model. Both the mean grain size L and Monte Carlo simulation time t_{MCS} are dimensionless in this figure.

The t_{MCS} values at different locations calculated from equation (6) cannot be directly applied in the MC algorithm. This is because the choice of grid point for updating orientation number is random in the MC technique, and thus the probability to select each grid point is the same in traditional MC calculations. However, grains must grow at higher rates in regions of higher temperature in the weld HAZ where a steep temperature gradient exists. This fact must be included in any realistic grain growth calculation scheme. One way to achieve this is to devise a scheme where grain orientations at higher temperature locations (higher t_{MCS} locations) are updated more frequently by considering a probability gradient [7]. In other words, the site selection probabilities vary with location to account for the variation of temperature in the HAZ. The larger the t_{MCS} at a site, the higher the corresponding site selection probability, $p(r)$:

$$p(r) = \frac{t_{MCS}(r)}{t_{MCSMAX}} \tag{7}$$

where $t_{MCS}(r)$ is the computed MC simulation time at the site with a distance r from the heat source and t_{MCSMAX} is the maximum MC simulation time. The site selection probability is different from the orientation change probability defined by equations (2) and (3). The orientation change probability is determined by the local interaction energy due to attempted reorientation. The site selection probability, on the other hand, biases more frequent selection of those sites that have high temperatures so that grains can grow faster at those locations.

4. RESULTS AND DISCUSSION

4.1. Temperature distributions and flow patterns

An example of the computed temperature and velocity fields in the weldment is shown in Fig. 1. The general features of the calculated temperature field are consistent with the results reported in the literature [13]. In front of the heat source, the temperature gradient is greater than that behind the source. The high temperature gradient results in slightly greater liquid metal velocities in front of the heat source than behind the source. On the surface of the weld pool, the liquid metal moves from the center to the periphery. This is expected for a metal with a very low concentrations of surface active elements such as sulfur and oxygen, and results in a negative temperature coefficient of surface tension $d\gamma/dT$. As the result of the outward fluid flow and convective heat transfer on the surface, the weld pool is wide and shallow.

In Table 4, the calculated temperatures and velocities from the turbulence model are compared with the results calculated assuming laminar heat transfer and fluid flow in the weld pool. It can be observed that the peak temperatures assuming laminar flow are unrealistically high. Calculations considering turbulence in the weld pool lead to reasonable values of temperatures and velocities.

4.2. Geometry of the FZ and the HAZ

A typical calculated fusion zone geometry is compared with the corresponding experimental results in Fig. 2. The calculated geometry of the fusion zone is

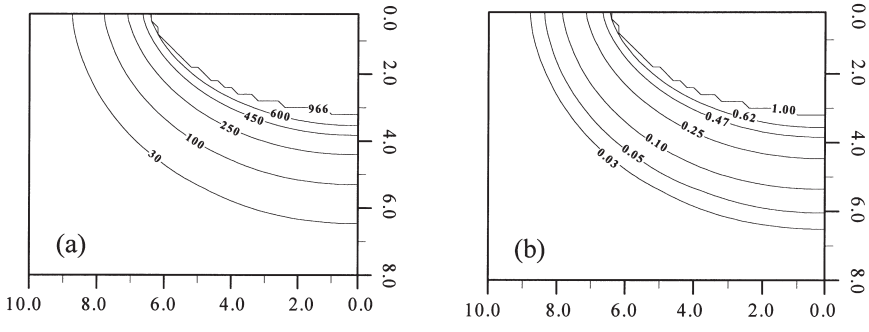

Fig. 4. (a) Spatial distribution of Monte Carlo simulation time t_{MCS} at $x = -12.0$ mm plane of the domain. (b) Spatial distribution of site selection probability at $x = -12.0$ mm plane.

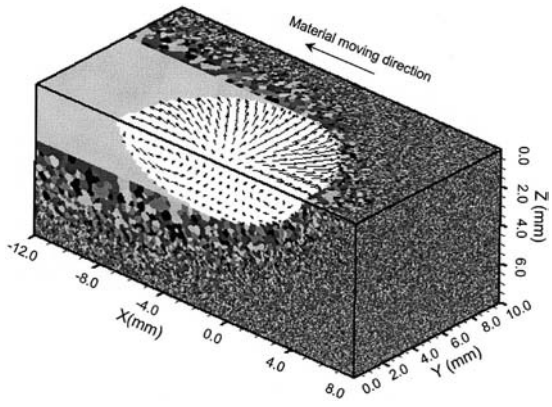

Fig. 5. Map of grain structure around the weld pool in three dimensions using 400×200×160 grids. The grid spacing is 50 μm. GTA welding with 108 A, 18.5 V and 1.0 mm/s welding speed.

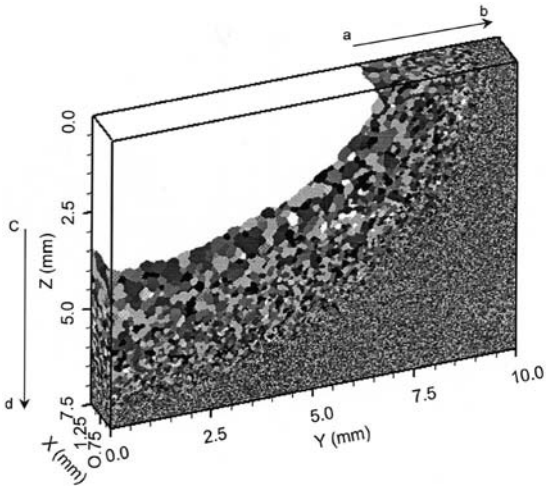

Fig. 7. Simulated final grain structure of the HAZ using 50×400×300 grids. GTA welding with 108 A, 18.5 V and 1.0 mm/s welding speed.

determined by the titanium liquidus temperature [35] (1941 K). Since the starting temperatures for the annealing and recrystallization of α-Ti are not precisely known, the geometry of the HAZ cannot be exactly predicted. However, the β phase containing region (α-Ti partially or fully transformed to β-Ti) in the HAZ can be predicted. This region exists between the α/β transition isotherm [35] (1158 K) and the liquidus temperature (1941 K) which have been experimentally measured [28] and modeled [30] for a heat input of 1998 J/mm. If we denote this β phase containing region as the HAZ, its width can be predicted. From Fig. 2(a), it can be observed that the calculated geometry of both the FZ and the HAZ obtained from the turbulent heat transfer and fluid flow model are comparable with the experimental results. It can also be observed that the widths of the HAZ at various locations are different. The width of the HAZ on the top surface is relatively smaller than that below the weld pool. The calculated dimensions of the HAZ from the turbulent model are comparable with the experimental data for various heat inputs. In contrast, there are significant differences between the experimental geometry and those calculated by assuming laminar heat transfer and fluid flow in the weld pool as shown in Fig. 2(b). Dimensions of the weld pool geometry presented in Table 5 show that the weld pool depths calculated from laminar calculation agree reasonably well at the lowest heat input but deviate significantly at higher heat inputs. The results show that turbulent calculations are more accurate, at least for high heat inputs.

4.3. Grain growth in the single-phase β region

4.3.1. Selection of simulated domain and grid spacing. In the present investigation, three dimensional MC simulations were carried out in a simple cubic lattice system. The total number of grain orientations, *q*, was taken to be 48 in the present simulation, since it is known [2] that the grain growth exponent becomes almost independent of *q* when its value is larger than 30. The local energy was calculated by a shell of 26 grid points consisting of the first, second, and third nearest neighbors. It should be pointed out that in the present MC model, the new attempted orientation was limited to one of the near-

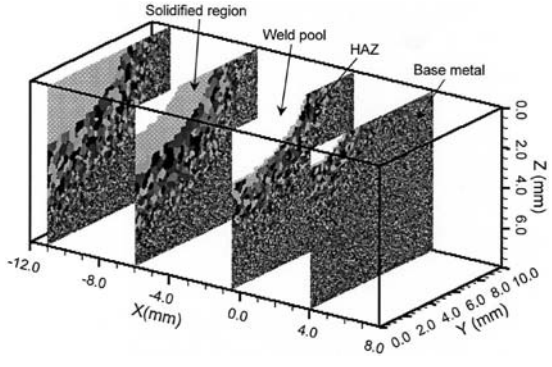

Fig. 6. Grain structure evolution as the material approaches and moves away from the heat source ($x = 0$). GTA welding with 108 A, 18.5 V and 1.0 mm/s welding speed.

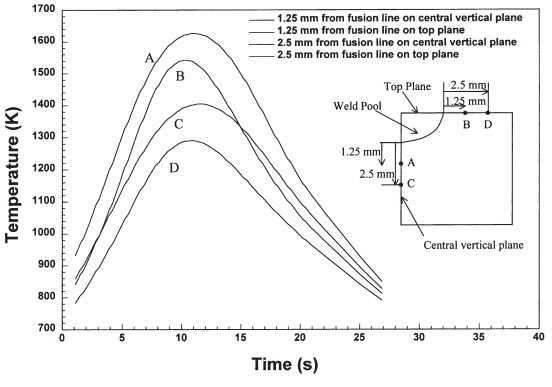

Fig. 8. Thermal cycles at different locations, 1.25 and 2.5 mm from the fusion plane for weld 2 (1998 J/mm).

Table 5. Comparison of the calculated weld pool dimensions from laminar and turbulent flow models with the experimental results[a]

	Laminar model				Turbulent model				Experimental	
	Depth		Width		Depth		Width		Depth	Width
Weld no.	*D* (mm)	Diff (%)	*W* (mm)	Diff (%)	*D* (mm)	Diff (%)	*W* (mm)	Diff (%)	(mm)	(mm)
1	1.8	43.7	14.7	10.5	3.4	6.3	13.6	2.3	3.2±0.2	13.3±0.3
2	1.6	40.7	14.1	17.5	2.8	3.7	12.2	1.6	2.7±0.2	12.0±0.3
3	1.4	22.2	12.3	16.0	1.9	5.6	10.8	1.9	1.8±0.2	10.6±0.2
4	1.0	16.7	9.9	22.2	1.5	25.0	9.1	12.3	1.2±0.2	8.1±0.2

[a] The symbols *D* and *W* represent the depth and width of the calculated weld geometry. Diff represents the relative difference between the calculated values and the corresponding experimental data.

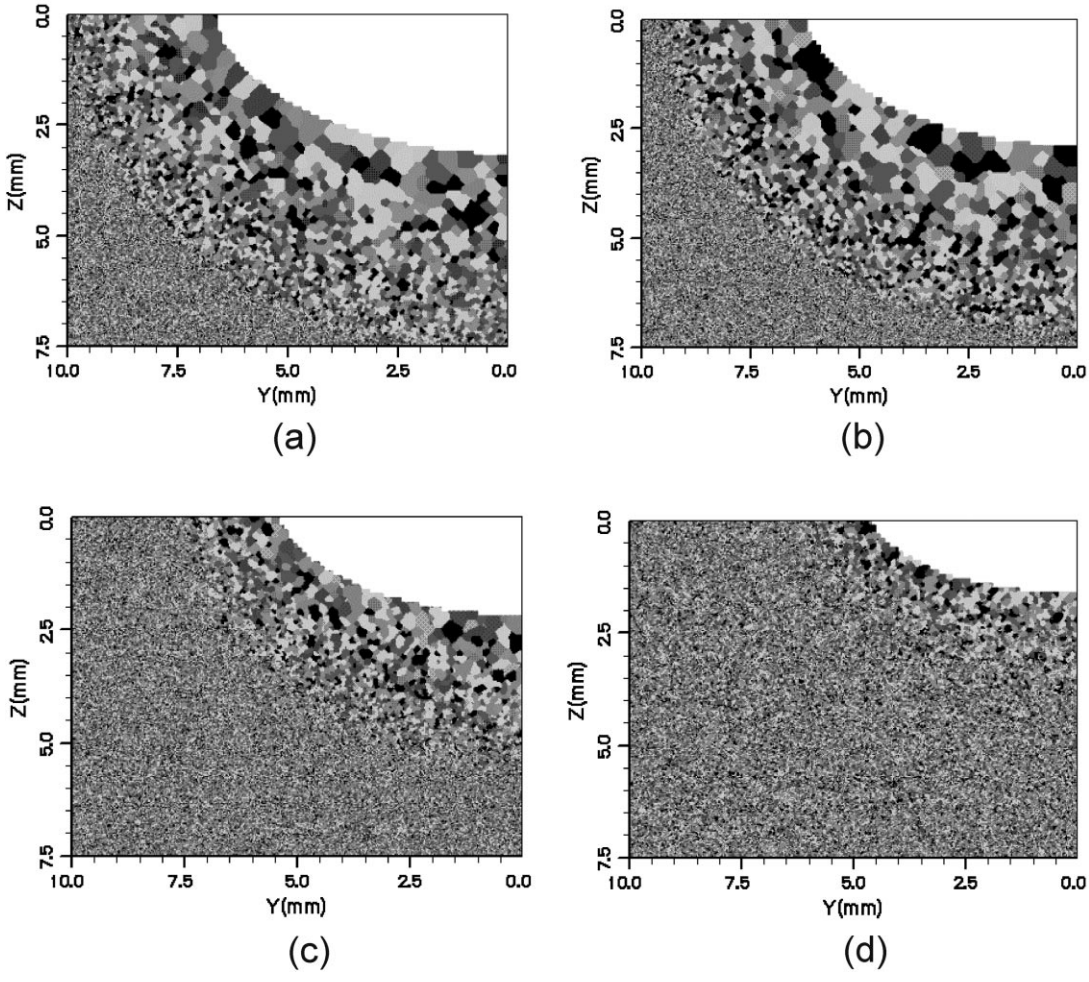

Fig. 9. Comparison of the simulated grain structures under various welding conditions: (a) weld 1 (3932 J/mm); (b) weld 2 (1998 J/mm); (c) weld 3 (1026 J/mm); (d) weld 4 (534 J/mm).

est-neighbor orientations rather than all possible orientations in the system. This is because the grain boundary migration only results from the process that atoms close to the grain boundary jump into the nearest grain interior. The soundness of this method has been justified in the literature [36].

Two domains in the weldment were selected in the present study. The first domain, $20\times10\times8.0$ mm^3, was chosen to simulate real-time grain structure evolution in the entire HAZ where β grain growth occurs. A $400\times200\times160$ grid system was used with a grid spacing (λ) of 50 μm. This value is twice that of the initial β-Ti mean grain size (25 μm). The second domain had a volume of $1.25\times10\times7.5$ mm^3. The grid system used in this domain was $50\times400\times300$, which amounted to a grid spacing of 25 μm. If the first domain in this investigation ($20\times10\times8$ mm^3) is mapped with 25 μm spacing, a $800\times400\times320$ grid system or approximately 102 million grid points would be needed. The memory requirement for this grid system considering 100 time steps is beyond that available in most modern workstations. Consequently, the grid spacing for the first domain was taken as twice the initial mean grain size. The large grid spacing (λ) will not significantly affect the final grain structure as long as the final grain sizes are much larger than the grid spacing. This is because the effect of grid spacing (λ) on the grain size has already been considered in equation (6). However, grid spacing larger than average initial grain diameter is not suitable for simulation of the grain structure in regions where the grain growth is rather limited. In the welds studied in this paper, the final grain sizes near the fusion line are 5 to 12 times larger than the grid spacing adopted in the first domain with 50 μm grid spacing. Therefore, this grid spacing is suitable for the simulation of grain growth under the present welding conditions.

4.3.2. Grain growth kinetics from MC simulation under isothermal conditions. Figure 3 shows a plot of $\log(L)$ vs. $\log(t_{mcs})$ representing the simulated isothermal dimensionless grain growth kinetics for the two grid systems at 1550 K, which is the average of the melting temperature (1941 K) and the α/β transition temperature (1158 K). The data used for calcu-

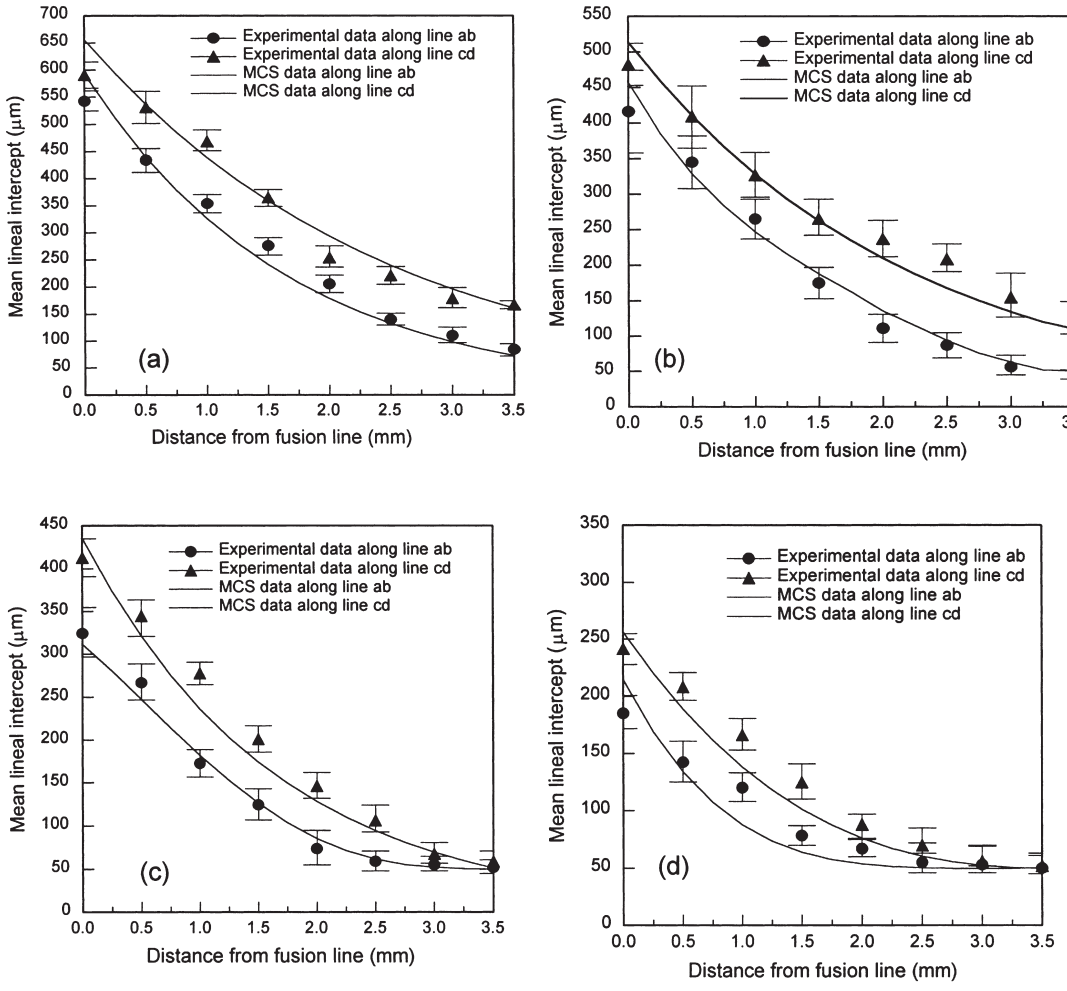

Fig. 10. Comparison of the simulated grain sizes with experimental measurements under various welding conditions: (a) weld 1 (3932 J/mm); (b) weld 2 (1998 J/mm); (c) weld 3 (1026 J/mm); (d) weld 4 (534 J/mm). The locations of the lines ab and cd are indicated in Fig. 7.

lations are presented in Table 3. It can be observed from this figure that the simulated grain growth kinetics in the two grid systems are the same, which indicates that the grids are sufficiently fine and the kinetics is independent of grid system chosen. The solid line in Fig. 3 is the result of a linear fit to the calculated results for both the grid systems. The values of K_1 and n_1 were determined from the slope and the intercept of the solid line to be 0.81 and 0.48, respectively. The grain growth exponent ($n_1 = 0.48$) is fairly close to the theoretical value of 0.50 and comparable with the value (0.46) reported in the literature [36] from 3D isothermal MC simulation. In order to achieve high numerical accuracy, the grid system chosen in the present 3D MC model (400×200×160) was much finer than that used (50×50×50) in the previous work.

4.3.3. Distributions of MC simulation step and site selection probability. After determining the constants K_1 and n_1 from the present 3D MC model, the t_{MCS} at each site was calculated from equation (6) by considering the thermal history of all the grid points. The distribution of the t_{MCS} in the first domain using a 400×200×160 grid system is shown in Fig. 4(a). From this figure, it can be observed that the maximum value of t_{MCS} lies at locations close to the fusion zone. It can also be observed from this figure that the value of t_{MCS} increases as the temperature or time for grain growth increases. After knowing the spatial distribution of t_{MCS} in the domain, the corresponding distribution of site selection probability, $p(r)$, in the cross section of the weld can be obtained from equation (7) as shown in Fig. 4(b). As expected, the spatial distribution of $p(r)$ is similar to that of t_{MCS}.

4.3.4. Simulated grain structure in the HAZ. The 3D map of grain structure distribution around the weld pool is shown in Fig. 5. The heat source is located at the position $x = 0.0$, $y = 0.0$ and $z = 0.0$. In front of the heat source ($x>0$), the material experiences significant grain growth during heating. This can be clearly observed in both the top surface and the symmetrical vertical plane. Behind the heat source

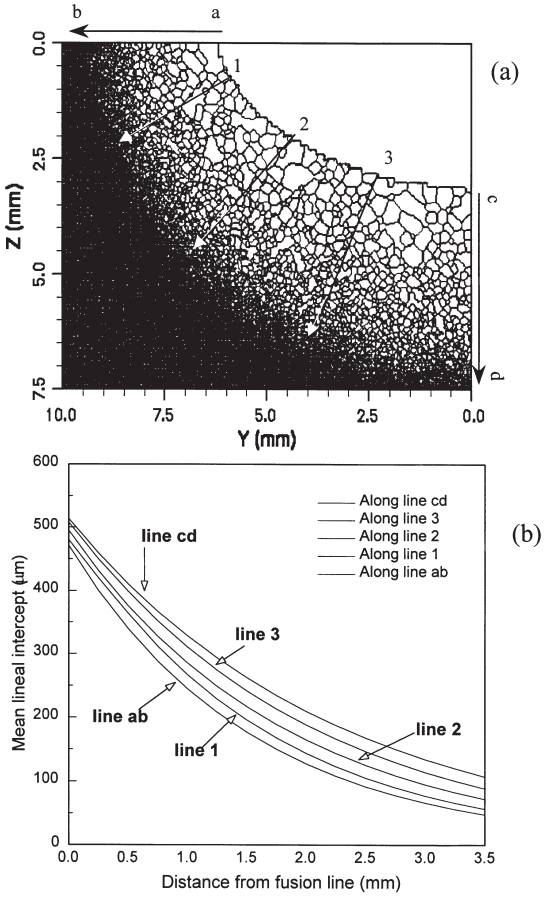

Fig. 11. Spatial distribution of grain size in the HAZ of weld 2 (1998 J/mm): (a) specified lines for grain size measurement; (b) grain size gradients along different lines.

($x<0$), the β-Ti grains are assumed to continue to grow until the temperatures reach the β/α transition temperature (1158 K). From the simulated 3D grain distribution map, the grain structure at all locations in the whole HAZ around the weld pool can be obtained. For example, the grain size distribution on the top surface and that on the symmetrical vertical plane can be clearly observed as shown in Fig. 5. In the simulated real-time grain structure map, the thermal effects on grain growth can be effectively illustrated. In the region in front of the weld pool, the extent of grain growth is limited and the grains are fine owing to the very short time available for grain growth prior to melting. In the solid region, the mean grain size becomes coarser with time.

The grain structure at any plane in the domain can be viewed by examining the corresponding cross sections normal to *x*, *y*, or *z* directions. Figure 6 shows the spatial distribution of grain structure at several cross sections normal to the *x* direction. The dynamic change of grain structure in the HAZ as well as the weld geometry is effectively illustrated in this figure. For example, it is observed that the extent of grain growth at a cross section 4 mm ahead of the heat source in the *x* direction is limited and only a very small portion of material melts at this location. The width of the weld pool continues to grow as a particular section of the material moves closer to the heat source.

The simulated final grain structure of the HAZ after the completion of welding is shown in Fig. 7. Significant spatial grain size gradient is observed in the simulated HAZ structure. The closer a site to the fusion line, the coarser is the grain size at that site. This is expected since the grain size change depends on both the temperature and the time period for grain growth. The higher the temperature for grain growth, the larger the final grain size. Furthermore, it can be observed that grain growth on the top surface of the HAZ (along line ab) is not as significant as that in the vertical direction shown by line cd in Fig. 7. This is because at any given time the temperature at the top surface is lower than in the interior of the weldment. This fact can be clearly observed in Fig. 8 where the thermal cycles at two equidistant locations, 1.25 mm and 2.5 mm from the fusion line, are shown. The temperatures at points A and C in the central vertical plane at any given time are much higher than those at points B and D on the top surface. Consequently the grain growth on the top surface is less pronounced than that below the weld pool. The simulated grain structures using a $50\times400\times300$ grid system for various welding conditions are shown in Fig. 9. The increase in the average grain size with the increase in heat input is clearly observed from this figure. Weld 1 has the largest heat input (3932 J/mm) and thus, it exhibits the most pronounced growth, while weld 4 with the lowest heat input (534 J/mm) exhibits relatively slow grain growth.

To verify the simulated results, the grain size distributions along both lines ab and cd, as shown in Fig. 7, were measured in all the welds. The experimental grain size measurement was made after cooling to ambient temperature. It should be noted that the grain size in the postweld microstructure is not the same as that predicted in the single β phase region due to β→α transformation occurring during cooling of the weldment. However, the prior β grain boundary can still be identified from the postweld microstructure [30]. The calculated results for the four welds are compared with the experimental results in Fig. 10. The lineal intercept method was used in both experimental measurements and theoretical calculations. It is observed that the calculated and the experimentally measured grain sizes are comparable in all four welds. Furthermore, at locations equidistant from the fusion plane, the mean grain sizes at various locations along line ab are smaller than those along line cd in all the welds. These results indicate the strong influence of time and temperature on the kinetics of grain growth.

Figure 11(a) and (b) show the spatial grain size variation for a cross sectional plane, $X = 1.5$ mm from the fusion line for weld 2. It can be observed that the mean grain sizes along lines ab, 1, 2, 3, and cd are 176 μm, 196 μm, 217 μm, 242 μm, and 262

μm, respectively. Thus, the grain size at the same distance from the fusion line increases progressively counter-clockwise along the circumferential direction, from line ab, line 1, line 2, line 3, and line cd. A similar behavior was also observed in planes perpendicular to the plane shown in Fig. 11(a). Thus, 2D calculations cannot adequately describe grain growth in the HAZ.

4.3.5. Grain size distribution. The measured average prior β grain size distribution at three planes parallel to the top surface, 0.5 mm, 1.5 mm, and 2.5 mm below the weld pool in weld 2, is compared with the corresponding computed values in Fig. 12(a), (b) and (c), respectively for weld 2 (1998 J/mm). In these figures, the experimental data are presented by histograms and the results of MC simulation are presented by solid dots. The experimentally determined prior β grain size distribution in the base metal is presented in Fig. 12(d) for comparison. It can be observed from Fig. 12 that the results from the 3D MC simulations are comparable with the experimental data. In each plane, the grain size distributions from both simulation and experimental data exhibit asymmetric peaks at $\log_{10}(R/R_{avg}) = 0$ and has an upper cut-off around $\log_{10}(R/R_{avg}) = 0.5$. This means that most of the grains in the domain have the average grain size and the maximum grain size is about 3.2 times the average grain size. These grain size distributions in the HAZ are consistent with those reported under isothermal conditions in the literature [3]. Comparing the grain size distributions at the three planes, it can be seen that the peak frequency changes with distance from the fusion plane. The closer the plane to the weld pool, the smaller the magnitude of the peak frequency. For example, the grain size distributions in the planes fairly close to the fusion plane, i.e. 0.5 mm and 1.5 mm below the weld pool, shown in Fig. 12(a) and (b), have lower frequency peaks and broader size distribution spectra. In contrast, the grain size distribution in the plane 2.5 mm below the weld pool, shown in Fig. 12(c), is comparable with that in the base metal presented in Fig. 12(d) because this plane is further from the fusion plane.

5. SUMMARY AND CONCLUSIONS

This paper reports the first 3D modeling of grain structure in the HAZ of GTA welded commercially

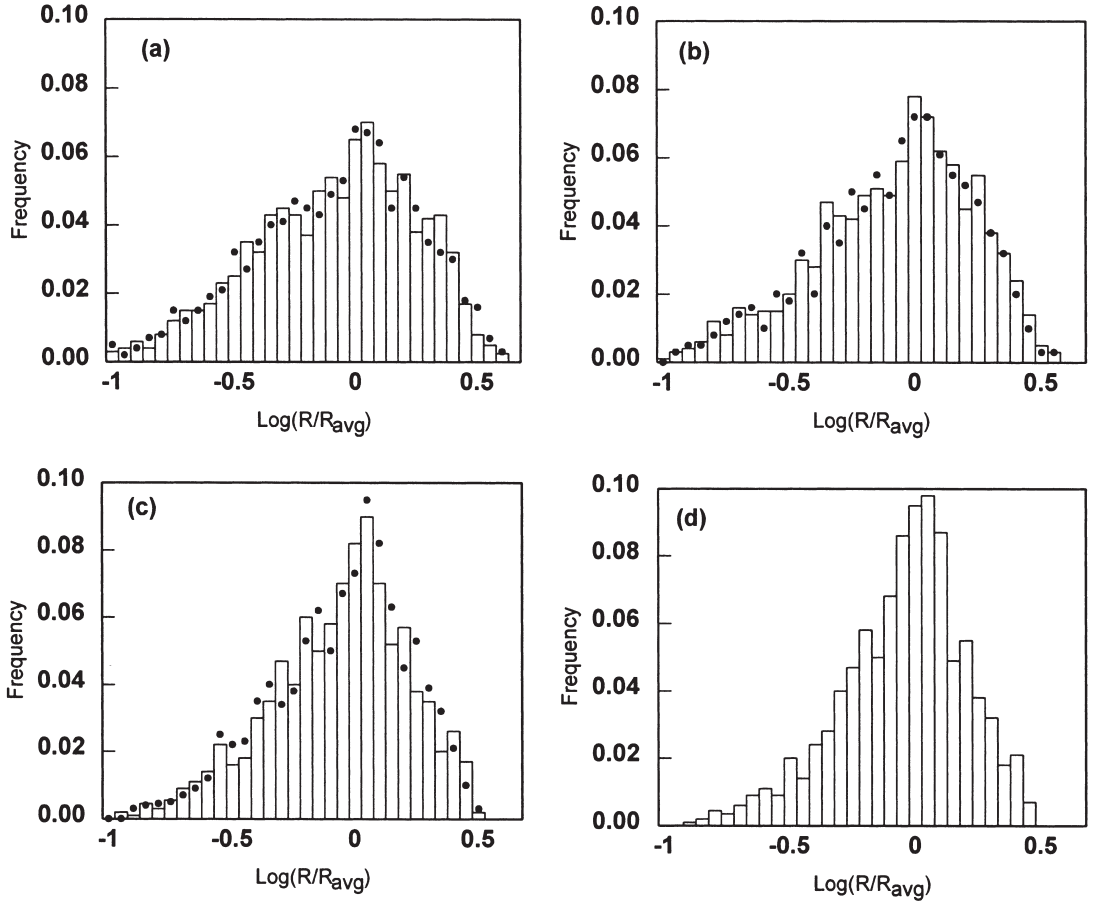

Fig. 12. Grain size distributions determined from experimental data (histograms) compared with the results from 3D MC simulation (solid dots) at different locations in weld 2 (1998 J/mm): (a) 0.5 mm from fusion line; (b) 1.5 mm from fusion line; (c) 2.5 mm from fusion line; (d) base metal.

pure titanium based on fundamentals of transport phenomena and grain growth theory. The grain structures in the HAZ under various welding conditions were simulated and compared with the corresponding experimental data. The agreement between the calculated and experimental results indicates significant promise for understanding of grain growth in titanium welds by this approach. Through a comparison of the calculated and experimental results, the following conclusions can be made.

1. The experimentally determined shape and size of the weld pool agreed well with the corresponding calculated values for all heat input conditions when turbulent flow was considered in the weld pool. However, the agreement for the laminar flow model was only good for the lowest heat input weld.
2. Both the measurements and the computed results showed that the average prior β grain size near the fusion plane was about five to 12 times larger than that in the base plate depending on the experimental conditions, and the grain size decreased continuously with distance from this plane. The extent of grain growth also increased with heat input.
3. The calculated grain sizes for various heat inputs were comparable with the corresponding experimental results. In particular, it was found that the grain size in the HAZ varied in regions equidistant from the fusion plane. The mean grain size in regions equidistant from the fusion plane increased along the circumferential direction from the top surface to the weld root. This behavior is consistent with higher temperatures in the interior of the weldment compared with the top surface at any given time. Furthermore, these results suggest that all the previous 2D calculations of grain size in the weld HAZ need to be reexamined.
4. The grain size distribution near the fusion zone was broader since the average grain size was larger in this region. The experimental grain size distribution function agreed well with the simulated results.

Acknowledgements—The Penn State portion of this research was supported by a grant from the US Department of Energy, Office of Basic Energy Sciences, Division of Materials Sciences, under grant number DE-FGO2-84ER45158. The LLNL portion of this research was performed under the auspices of the US Department of Energy, Lawrence Livermore National Laboratory, under Contract No. W-7405-ENG-48. The authors would like to express their gratitude to Mr Kershaw of LLNL for optical metallography.

REFERENCES

1. Gao, J. and Thompson, R. G., *Acta Metall.*, 1996, **44**, 4565.
2. Anderson, M. P., Srolovitz, D. J., Grest, G. S. and Sahni, P. S., *Acta Metall.*, 1984, **32**, 783.
3. Srolovitz, D. J., Anderson, M. P., Sahni, P. S. and Grest, G. S., *Acta Metall.*, 1984, **32**, 793.
4. Saito, Y. and Enomoto, M., *ISIJ Int.*, 1992, **32**, 267.
5. Grest, G. S., Srolovitz, D. J. and Anderson, M. P., *Acta Metall.*, 1985, **33**(3), 509.
6. Gao, J., Thompson, R. G. and Cao, Y., in *Trends in Welding Research*, eds. H. B. Smartt, J. A. Johnson and S. A. David, ASM International, Materials Park, OH, 1996, p. 199.
7. Radhakrishnan, B. and Zacharia, T., *Metall. Mater. Trans. A*, 1995, **26A**, 2123.
8. Wilson, A. L., Martukanitz, R. P. and Howell, P. R., in *Trends in Welding Research*, eds. J. M. Vitek, S. A. David, J. A. Johnson, H. B. Smartt and T. DebRoy, ASM International, Materials Park, OH, 1998, p. 161.
9. DebRoy, T. and Kou, S., *Welding Handbook*, chapter 3, in press.
10. David, S. A. and DebRoy, T., *Science*, 1992, **257**, 497.
11. DebRoy, T. and David, S. A., *Rev. Mod. Phys.*, 1995, **67**, 85.
12. Oreper, G. M. and Szekely, J., *J. Fluid Mech.*, 1984, **147**, 53.
13. Kou, S. and Wang, Y. H., *Metall. Trans. A*, 1986, **17A**, 2265.
14. Choo, R. T. C., Szekely, J. and David, S. A., *Metall. Trans. B*, 1992, **23B**, 371.
15. Chan, C., Mazumder, J. and Chen, M. M., *Metall. Trans. A*, 1984, **15A**, 2175.
16. Mundra, K., DebRoy, T. and Kelkar, K., *Numerical Heat Transfer*, 1996, **29**, 115.
17. Pitscheneder, W., DebRoy, T., Mundra, K. and Ebner, R., *Weld. J.*, 1996, **75**(3), 71s.
18. Mundra, K., Blackburn, J. M. and DebRoy, T., *Sci. Technol. Weld. Join.*, 1997, **2**(4), 174.
19. Block-Bolten, A. and Eager, T. W., *Metall. Trans. B*, 1984, **15B**, 461.
20. Khan, P. A. A. and DebRoy, T., *Metall. Trans. B*, 1984, **15B**, 641.
21. Mundra, K., DebRoy, T., Babu, S. S. and David, S. A., *Weld. J.*, 1997, **76**(4), 163s.
22. Yang, Z. and DebRoy, T., *Sci. Technol. Weld. Join.*, 1997, **2**(2), 53.
23. Yang, Z. and DebRoy, T., *Metall. Trans. B*, 1999, **30B**, 483.
24. Malinowski-Brodnicka, M., DenOuden, G. and Vink, W. J. P., *Weld. J.*, 1990, **69**, 52s.
25. Choo, R. T. C. and Szekely, J., *Weld. J.*, 1994, **73**(2), 25s.
26. Hong, K., Weckman, D. C. and Strong, A. B., in *Trends in Welding Research*, eds. H. B. Smartt, J. A. Johnson and S. A. David, ASM International, Materials Park, OH, 1996, p. 399.
27. Aboav, D. A. and Langdon, T. G., *Metallography*, 1969, **2**, 171.
28. Elmer, J. W., Wong, J. and Ressler, T., *Metall. Mater. Trans. A*, 1998, **29A**(11), 2761.
29. Annual Book of ASTM Standards, 1996, vol. 1, sect. 3, ASTM, West Conshohoken, PA.
30. Yang, Z., Elmer, J. W., Wong, J. and DebRoy, T., *Weld. Res. Suppl.*, 2000, **79**(4), 97s.
31. Gill, X., Rodriguez, D. and Planell, J. A., *Scripta Metall. Mater.*, 1995, **33**, 1361.
32. Porter, A. and Easterling, K. E., *Phase Transformation in Metals and Alloys*. Chapman and Hall, London, 1992.
33. de Reca, N. E. W. and Libanati, C. M., *Acta Metall.*, 1968, **16**, 1297.
34. *Titanium Alloys*, ASM International, Materials Park, OH, 1994.
35. Donachie, M. J. Jr, *Titanium: A Technical Guide*, ASM International, Materials Park, OH, 1994, p. 177.
36. Radhakrishnan, B. and Zacharia, T., *Metall. Mater. Trans. A*, 1995, **26A**, 167.